energies

MDPI

Article

A Fast Converter Synchronization Speed Method Based on the Frequency Difference on Both Sides of the Grid Connection Point

Jiangang Lu [1], Haobin Li [1], Feng Liao [1,*], Yuhui Huang [1] and Xialin Li [2]

[1] Guangdong Power Grid Co., Ltd., China Southern Power Grid Co., Ltd., Guangzhou 510050, China
[2] School of Electrical and Information Engineering, Tianjin University, Tianjin 300072, China
* Correspondence: liaofeng137@126.com

Abstract: The challenge of achieving a reliable and safe synchronization process for microgrids under weak communication conditions is a significant issue in distributed grid-connected energy storage. This is also the core motivation of this study. First, the concept of weak communication is introduced, and weak communication conditions are simulated by limiting the number of communications. Additionally, a fast synchronization method based on the frequency difference at the grid connection point is proposed, which allows for the rapid synchronization of converters under weak communication conditions. This method also includes an analysis of the range for key parameters, providing practical and feasible guidance for its real-world application. Finally, the validity of the theory is verified through PSCAD/EMTDC simulations and physical experiments.

Keywords: synchronization method; weak communication conditions; networked control

Citation: Lu, J.; Li, H.; Liao, F.; Huang, Y.; Li, X. A Fast Converter Synchronization Speed Method Based on the Frequency Difference on Both Sides of the Grid Connection Point. *Energies* **2024**, *17*, 5639. https://doi.org/10.3390/en17225639

Academic Editors: José Matas and Kwok Tong Chau

Received: 3 August 2024
Revised: 10 September 2024
Accepted: 7 November 2024
Published: 11 November 2024

1. Introduction

To accelerate the transformation of the energy structure, the penetration of renewable energy sources, represented by photovoltaics and wind power, into the power grid has rapidly increased [1–3]. Grid-forming control, which uses self-excited angle control, serves as a crucial interface between renewable energy sources and the power grid [4,5]. It plays a significant role in the stable operation of microgrid systems [6] and has been widely studied and applied, such as through the use of virtual synchronous generators (VSGs) that can simulate synchronous generators [7–9]. When grid-forming control needs to be integrated into the main grid, a pre-synchronization process is often required [10]. Under weak communication conditions, the system's synchronization and grid connection process can be affected, making it difficult for the system to quickly adjust its frequency and phase angle. This impacts the reliability of the grid connection, leading to synchronization failures and preventing the system from switching to grid-connected operation, which may even affect the stable operation of the system. Therefore, improving the synchronization speed and ensuring a safe and reliable grid connection under weak communication conditions is of great importance, which is the primary motivation of this paper.

The large-scale integration of distributed energy resources can easily lead to issues such as voltage limits being exceeded in the grid [11]. Therefore, when energy storage systems based on grid-forming control need to be connected to the grid, synchronization is required to eliminate inrush currents caused by potential deviations in the voltage amplitude and initial phase. This ensures that the phase and amplitude of the system's output voltage are synchronized with the grid voltage before switching [12,13].

For synchronization in energy storage systems using networked control, the author of [14] designed a synchronization method without a phase-locked loop (PLL), which reduced the inrush current during the grid connection of VSGs, achieving a smooth no-load grid connection in the VSGs. However, this method is not suitable for VSGs under load

conditions and also requires relatively good communication conditions. The author of [15] designed a new phase angle input variable and proposed a smooth synchronization method for VSGs based on this variable. However, this method changes the control structure of VSGs, causing them to lose frequency support capability and the advantages of networked control. In [16], the author converted the phase angle into virtual power and proposed a synchronization method based on virtual power, achieving smooth grid connection in the energy storage system. However, this method increases the synchronization time and requires a more complex algorithm, making it difficult to implement in practical engineering. For synchronization methods under weak communication conditions, in [17], the author proposed a microgrid synchronization control strategy, achieving smooth switching between the microgrid and the grid without communication. However, this method is only applicable to a specific inverter control strategy, making it difficult to generalize. Reference [18] proposes a control strategy for systems equipped with battery energy storage and photovoltaics that achieves a smooth transition between the grid-connected mode and islanding mode by combining current control with voltage control. However, this method may cause an excitation surge and distorted voltage during switching, and it cannot be used under weak communication conditions. In [19], an author proposes a sensorless capacitance current control strategy based on observers. In the grid-connected mode, the outer loop of the grid connection is combined with droop control to form a composite control structure conducive to mode switching. However, the reference value of the capacitor voltage depends on islanding detection, which may compromise power quality. Moreover, this overly complex structure is not conducive to stable and smooth system-wide switching, and it also relies on certain communication conditions. Due to the complexity of the structure and algorithm, its practicality and economy in actual engineering are poor.

The main contributions of this paper are summarized as follows:

- A fast synchronization method was proposed that increases the frequency difference between the grid connection points. Weak communication conditions were simulated by limiting the number of communications between the MGCC and VSCs. The effectiveness of the proposed method under weak communication conditions was validated through PSCAD/EMTDC simulations and physical experiments.
- The parameter selection method for the proposed approach was detailed, including the range of values. This provides practical and feasible guidance for the real-world application of the method.

2. Typical Networked Voltage Source Converter (VSC)

In this context, WG refers to a weak grid, typically represented by the short-circuit ratio (SCR) [20]. The definition of a weak grid is similar to that in references [21,22], where a short-circuit ratio of 0–10 is considered weak. In both the simulation and physical experiments presented in this paper, the SCR is set to 2. A typical WG-VSC system is depicted in Figure 1. In the diagram, L_f, C_f, R_f, and L_g represent the LCL filter inductance, filter capacitance, filter inductance on the grid side only, and the grid impedance, respectively. V_{inv} denotes the converter terminal output voltage; PCC stands for the point-of-common-coupling control switch, controlled by the microgrid central controller (MGCC); and u_{vsg} and i_{vsg} are the voltage and output current at the VSG grid connection point, respectively. Q_{ref} and Q_{vsg} represent the reactive power reference value and actual output value of the energy storage inverter, with k_q as the reactive power droop coefficient, U_0 as the rated voltage value, U_{com} as the compensation voltage issued by the MGCC, and U_{ref} as the voltage magnitude reference value inputted to the dual-loop control. P_{ref} and P_{vsg} denote the active power reference value and actual output value of the energy storage inverter, respectively. ω_{com} is the phase angle compensation value issued by the MGCC, ω_0 is the rated angular frequency value, ω_{vsg} is the self-excitation generation angular frequency reference value, and θ_{vsg} is the angular frequency reference value inputted to the dual-loop control.

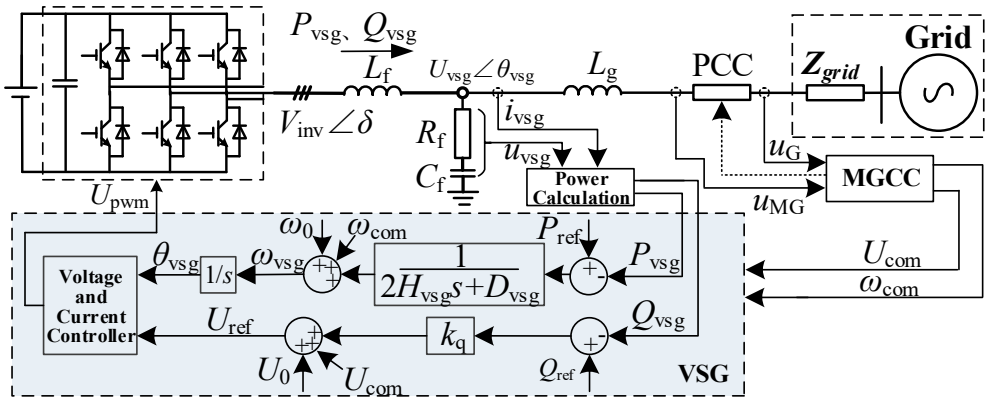

Figure 1. Typical WG-VSC system.

The relationship between the output frequency and active power output of the energy storage inverter using VSG technology in Figure 1 can be described as follows:

$$\omega_{vsg} = \omega_0 + \omega_{com} + (P_{ref} - P_{vsg})/(2H_{vsg}s + D_{vsg}) \quad (1)$$

where H_{vsg} and D_{vsg} represent the virtual inertia parameter and virtual droop parameter, respectively, in the virtual synchronous control.

$$U_{ref} = U_0 + U_{com} + k_q(Q_{ref} - Q_{vsg}) \quad (2)$$

where k_q represents the reactive power droop parameter. When an energy storage inverter using networked control needs to be integrated into an existing power grid, the MGCC simultaneously measures the voltages on both sides of the PCC grid connection switch and calculates the corresponding phase angle through the phase-locked loop. It then generates compensation values through the respective controllers. Once the voltage magnitudes and phase angles on both sides of the grid connection point meet the preset values, the PCC grid connection switch can be closed to integrate the entire system into the grid.

3. Fast Synchronization Grid Connection Method

In this section, we propose a fast synchronization and grid connection strategy based on actively increasing the frequency difference on both sides of the grid connection point. This strategy enables a fast grid connection speed under weak communication conditions, ensuring the safe and reliable grid connection of the overall system. Building upon this, we provide the principles and ranges for selecting relevant control parameters.

3.1. Fast Synchronization Strategy

Due to the asynchrony between voltage magnitudes and initial phase angles, a synchronization process is often necessary during the integration of energy storage microgrids into the grid, aimed at eliminating the occurrence of inrush currents. However, in practical applications, weak communication conditions such as significant communication delays, limited communication bandwidth, device loss, or communication failure may adversely affect synchronization effectiveness. This may render active synchronization strategies disadvantageous for system stability, especially in microgrids composed of multiple converter units, when coordinated control is applied for grid integration. Furthermore, frequent adjustments in voltage magnitudes and phase angles in microgrids constructed with power electronic devices might affect the electrical equipment within the system. Therefore, in such specific scenarios, passive synchronization methods may be preferable. Typically, in networked control, secondary control compensates for voltage and frequency deviations induced by droop control [12], resulting in minimal differences in voltage and phase angles at the grid connection point. Consequently, relying on frequency differences to passively

wait for the voltage at the grid connection point to meet grid requirements [23] may result in excessively long and uncertain synchronization times. Hence, we propose a simple fast synchronization method. This method detects the voltage and frequency at both ends and selectively compensates for the microgrid voltage under specific conditions. If the frequency difference at both ends is small, it actively adjusts the microgrid frequency to increase the frequency difference, facilitating a fast realignment of voltages at both ends. This synchronization method imposes minimal requirements on system communication conditions and allows frequency and voltage adjustments at a lower frequency, thereby reducing the impact on electrical devices within the microgrid system. The switch automatically closes when the voltages at both ends of the grid connection point meet the preset values, enabling synchronous grid integration. A schematic of the synchronization process is illustrated in the following diagram.

In the Figure 2, U_{MG}, θ_{MG}, and $f_{MG,}$ respectively, represent the voltage magnitude, phase angle, and frequency on the microgrid side, while U_G, θ_G, and f_G represent the voltage magnitude, phase angle, and frequency on the grid side. The method detects voltage and frequency at both ends. $f_{presets}$ is the preset frequency difference value, and $k_{p\_u\_com}$ and $k_{i\_u\_com}$ are the control parameters of the voltage compensation algorithm. U_{com} is the compensation value obtained by calculating the voltage magnitude difference on both sides and applying the compensation algorithm. It can be implemented through different controllers. In this paper, a PI algorithm is adopted, as shown in Equation (3).

$$\begin{gathered} U_{com} = k_{p\_u\_com}(U_G - U_{MG}) + (U_G - U_{MG})k_{i\_u\_com}/s \\ f_{com} = f_G - f_{MG} - f_{preset} \\ \omega_{vsg} = 2\pi f_{com} \end{gathered} \tag{3}$$

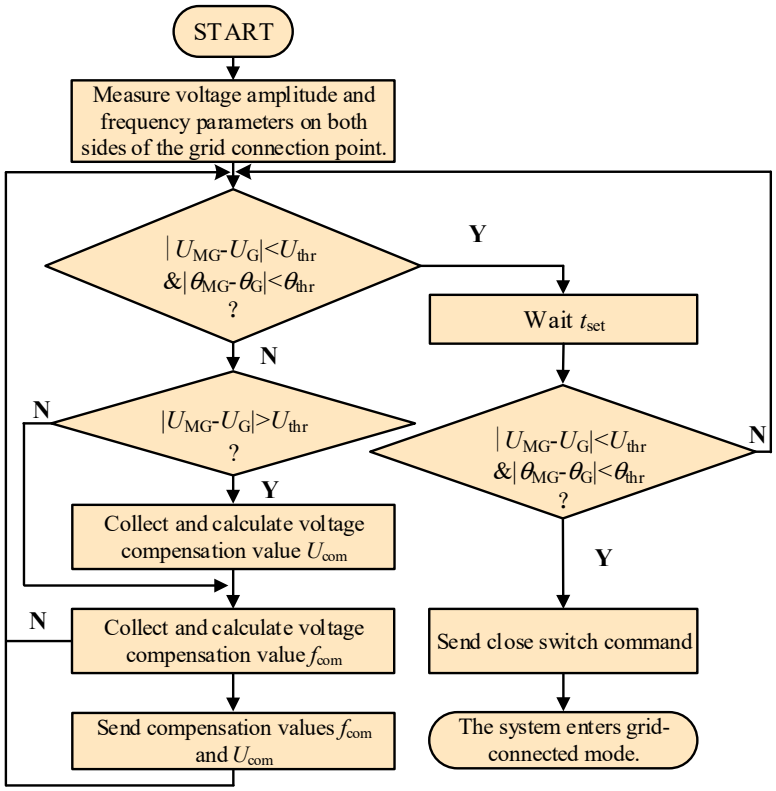

Figure 2. Flowchart of fast synchronization method.

The calculation method for the frequency compensation value at this time is as shown in the following Algorithm 1:

Algorithm 1: Calculate the voltage compensation value, U_{com}, and the phase angle compensation value, f_{com}

Input: Grid-side voltage frequency f_G; inverter-side voltage frequency U_G; grid-side voltage amplitude U_G; inverter-side voltage amplitude U_{MG}; preset frequency deviation $f_{presets}$; successful grid connection voltage threshold U_{thr}; successful grid connection phase angle threshold θ_{thr};
Initialization: $f_G = 0, f_{MG} = 0$; $U_G = 0$, $U_{MG} = 0$; $f_{preset} = 0.3$;
Calculation: (1) Obtain variables f_G, f_{MG}, U_G, and U_{MG} through the phase-locked loop (PLL) of the MGCC;
(2) Calculate the voltage compensation value using Equation (3) and perform voltage compensation.
(3) Calculate the synchronous compensation:
if $|f_G - f_{MG}| < f_{preset}$
    Calculate the frequency compensation value using Equation (3), and perform frequency compensation.
else
    Directly perform synchronous condition assessment.
(4) Synchronous condition assessment:
if (($|\theta_G - \theta_{MG}| < \theta_{thr}$) and ($|U_G - U_{MG}| < U_{thr}$))
    Close the grid connection switch and reset the synchronous control variables;
else
    Reperform step (1);
end
Output: Voltage compensation quantity, U_{com}; phase angle compensation quantity, f_{com}.

In practical scenarios, voltage amplitude adjustment can be achieved not necessarily through this method but by directly regulating the power source at the microgrid side, such as through adjusting the rated voltage of the inverter using grid-forming control. In actual adjustment processes, since phase angle adjustment requires higher frequency and precision, it often consumes more communication resources. In this method, if the actual communication conditions are poor, only one frequency compensation value can be sent, increasing the frequency difference between the microgrid side and the grid side to the preset value. Therefore, the fast method proposed in this paper does not require excessive communication resources and has minimal impact on the system from communication delays.

3.2. Principles for Selecting Parameters in Fast Synchronization Algorithms

In this paper, there are two main control parameters involved: one is the active frequency deviation, and the other is the grid-connecting frequency threshold during grid connection. Below, a conservative selection method will be proposed.

The default assumption is that the grid-side frequency at the point of connection is higher than the microgrid-side frequency. The principle of this value selection method is to use a fast synchronization algorithm to maintain the preset frequency difference between the grid side and the microgrid side while ensuring that the phase angle difference remains below the threshold value during the preset waiting time, t_{set}, thus meeting the grid connection requirements.

The specific principle is illustrated in Figure 3. In the figure, $\omega_{presests}$ represents the preset frequency difference. u_{MG1} and u_{G1} are the microgrid-side voltage and grid-side voltage that meet the grid connection requirements, respectively, while U_{MG2} and U_{G2} are the microgrid-side voltage and grid-side voltage after the waiting time, t_{set}.

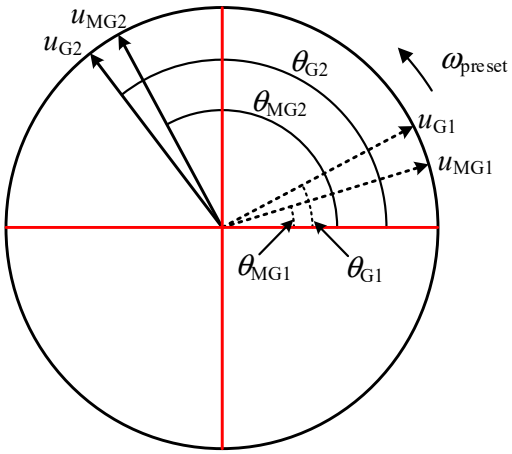

Figure 3. Parameter selection principle diagram.

At time t_1, the phase angle difference, θ_1, between the two sides of the connection point is as shown in Equation (4). At this moment, θ_{MG1} and θ_{G1} are the grid phase angle and microgrid phase angle that meet the threshold, respectively, as shown by the black dashed line. After time t_{set}, at time t_2, the phase angle difference becomes θ_2, as shown in Equation (4). At this time, θ_{G2} and θ_{MG2} are the grid phase angle and microgrid phase angle at time t_2. To meet the grid connection requirements, θ_2 should be less than θ_{thr}. Therefore, the corresponding value range can be calculated based on the relationship between the phase angle and frequency. Note that the phase angle values in the figure are only to illustrate the value range and do not represent the actual value range. The relationships between other variables in the figure are shown in Equation (5).

$$\begin{gathered} |\theta_{G1} - \theta_{MG1}| = \theta_1 \\ |\theta_{G2} - \theta_{MG2}| = \theta_2 \\ \theta_1 \leq \theta_{thr} \end{gathered} \tag{4}$$

$$\begin{gathered} t_1 - t_{et} = \theta_2 \\ \omega_{preset} = 2\pi f_{preset} \end{gathered} \tag{5}$$

For setting the synchronization preset threshold value for voltage U_{thr}, it can be determined based on actual requirements. For instance, when there are power electronic devices sensitive to transient currents in the system, U_{thr} can be set to 5V. As for the phase angle threshold θ_{thr}, it can be related to the waiting time t_{set} and the preset phase angle threshold as follows. If the system needs to be successfully grid-connected, θ_{thr} should satisfy the following relationship:

$$\omega_{preset} \leq \theta_{thr}/(t_{set}) \tag{6}$$

According to the reference grid-connecting values provided in [24], taking t_{set} = 0.05 s, $\theta_{thr} \leq 0.1$ rad and U_{thr} = 5 V, we can calculate $f_{preset} \leq 0.318$ Hz. Additionally, $t_{set} \leq 0.05$ s. Therefore, we used the following simulation and physical experiment parameters: f_{preset} = 0.3 Hz, θ_{thr} = 0.1 rad and U_{thr} = 5 V.

When the frequency at the grid side of the connection point is lower than that at the microgrid side, i.e., $f_G < f_{MG}$, it can be seen from Equation (3) in this paper that f_{com} will be less than 0. This value is sent from the MGCC to the VSC, which will reduce the microgrid frequency and increase the frequency difference to f_{preset}, achieving the same conditions as when the grid-side frequency is higher than the microgrid-side frequency. This means that the relative magnitude of the frequencies at the connection point does not affect the formation of the frequency difference and does not impact the effectiveness of the proposed accelerated synchronization method.

At the same time, when multiple microgrid synchronous generators are connected to the same grid and the grid's impedance is relatively high, certain disturbances may indeed lead to instability. In such cases, the method should be adjusted. If there are n machines with good communication conditions, these n machines can be grouped together to use this method for grid integration. For machines with significant communication delays between them, this method can be applied individually to each machine for synchronization.

Finally, if the phase angles and voltage magnitudes on both sides of the grid connection point are similar and the grid frequency experiences a sudden drop, let the grid frequency drop to f_{G_p} and the microgrid frequency be f_{MG_p}, with a preset frequency difference of f_{preset_p}. Define $\omega_{G\_p} = 2\pi f_{G\_p}$ and $\omega_{MG\_p} = 2\pi f_{MG\_p}$. If $|\omega_{G\_p} - \omega_{MG\_p}| \leq \theta_{thr}/t_{set}$, the microgrid can still be integrated into the system. However, if $|\omega_{G\_p} - \omega_{MG\_p}| > \theta_{thr}/t_{set}$, it will result in the MGCC detecting that the phase angles on both sides cannot meet the requirements, indicating that the microgrid cannot meet the integration conditions and cannot be integrated into the system. While there is indeed such a risk, given the parameters set, if f_{MG} was 49.7 Hz, the grid frequency, f_G, would need to drop from 50 Hz to 49.182 Hz or rise to 50.318 Hz. The system's grid frequency is typically considered to be within ±0.2 Hz, and if the system capacity is smaller, this can be relaxed to ±0.5 Hz [25]. Therefore, unless there is an extremely severe drop in the system frequency, the method proposed in this paper should be applicable in most operating conditions.

4. Simulation Cases and Physical Experiment Validation

In this section, a PSCAD/EMTDC electromagnetic transient simulation case and a physical experiment platform were set up to validate the fast synchronization grid connection strategy proposed, as discussed in Section 3.

4.1. Simulation Validation

To validate the effectiveness of the proposed fast synchronization method, a grid-connected simulation platform and a physical experiment platform were constructed using a single inverter, and simulations and physical experiments were conducted for both fast synchronization and passive synchronization. In passive synchronization as shown in Figure 4, no compensation values are sent. Instead, the MGCC collects the voltages on both sides of the grid connection point and obtains the frequency and phase angle through phase locking. When the grid connection conditions are met, a grid connection command is immediately issued to transition the entire system to grid-connected operation. When using the accelerated synchronization algorithm, compensation values need to be computed internally in the MGCC and then sent to each inverter through the communication channel to adjust the phase angle. In both the simulations and experiments, the setup was configured so that the MGCC and VSCs could communicate only once, after which the communication line was disconnected, and no further communication between the MGCC and VSCs occurred. This was carried out to simulate weak communication conditions. The specific circuit diagram for the simulation is shown in Figure 4, and the experimental parameters are listed in Table 1.

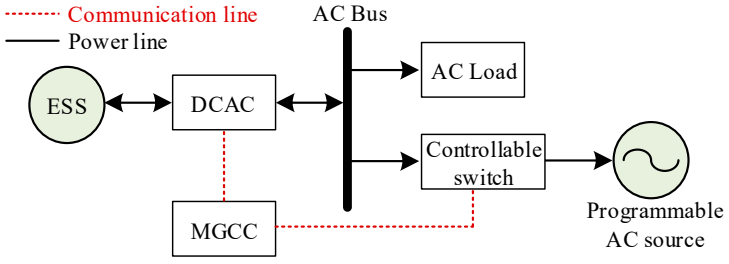

Figure 4. Simulation experiment circuit diagram.

Table 1. Main functions of each part of the system.

Module	Parameters	Symbols	Data
MGCC	Voltage synchronization control parameters	k_{p_vo}, k_{i_vo}	0.3, 5
	Voltage synchronization threshold	U_{thr}	5 V
	Phase angle synchronization threshold	θ_{thr}	0.1 rad
	Sampling period	$T_{s\_DC/DC}$	66.67 µs
DCAC	Normalized power	P_{acB}	50 kW
	Parameters for virtual synchronous control primary frequency regulation	D_{vsg}	50
	Parameters for virtual synchronous control virtual inertia	H_{vsg}	1
	Processing period	T_{s_DCAC}	66.67 µs

The simulation results are shown in the Table 2 below:

Table 2. Simulation results.

Simulation Conditions	AC Load	Time for Passive Synchronization	Time for Fast Synchronization	Acceleration Ratio
Simulation Conditions 1	0	>20 s	2.80 s	-
Simulation Conditions 2	$0.05P_{acB}$	14.38 s	2.49 s	82.7%
Simulation Conditions 3	$0.10P_{acB}$	6.83 s	2.17 s	68.3%
Simulation Conditions 4	$0.15P_{acB}$	3.58 s	1.84 s	48.6%
Simulation Conditions 5	$0.20P_{acB}$	2.23 s	1.51 s	31.9%

From the results, we can observe the following:

(1) When the synchronization control parameters are the same and there is basically no initial frequency difference, as shown in simulation condition 1, using the passive synchronization method takes a longer time to synchronize, whereas employing the proposed fast synchronization method significantly reduces the synchronization time.

(2) For smaller initial frequency differences, such as in simulation conditions 2 to 3, when the frequency difference is around 0.05 Hz, the synchronization time with the proposed fast method is only 17.3% compared to the conventional passive synchronization method. When the frequency difference is around 0.1 Hz, the synchronization time is 31.7%, demonstrating a substantial reduction in synchronization time with the proposed fast method.

(3) As the frequency difference increases, the effectiveness of the fast synchronization method gradually diminishes. For example, in simulation conditions 4 to 5, when the frequency difference is 0.15 Hz, the fast method takes 51.4% of the time compared to the conventional passive synchronization method, and when the frequency difference is 0.2 Hz, the fast method only takes 78.1% of the time. Thus, the effectiveness of the proposed fast synchronization method is more pronounced when the frequency difference between the two sides of the grid connection point is smaller. This is because when the frequency difference between both sides of the grid connection point is large, the time required for the voltages on both sides to coincide is very short. Therefore, in such scenarios, the time needed for the passive synchronization algorithm is minimal,

and the advantage of using an accelerated synchronization algorithm becomes less apparent. However, there are associated risks. Specifically, although the phase angle difference may be within the threshold, due to the large frequency difference between both sides of the grid connection point, the phase angle difference might exceed the threshold after the waiting time, t_{set}. In this case, the synchronization requirements cannot be met. However, the accelerated synchronization algorithm will not encounter this issue.

4.2. Physical Experiment Validation

To validate the effectiveness of the algorithm proposed in this paper, energy storage was simulated using a DC source, and a bidirectional DC-AC converter was used as the interface converter. The grid was simulated using an AC source. Following the simulation case shown in Figure 5, a physical experimental platform was set up as shown in Figure 5 below:

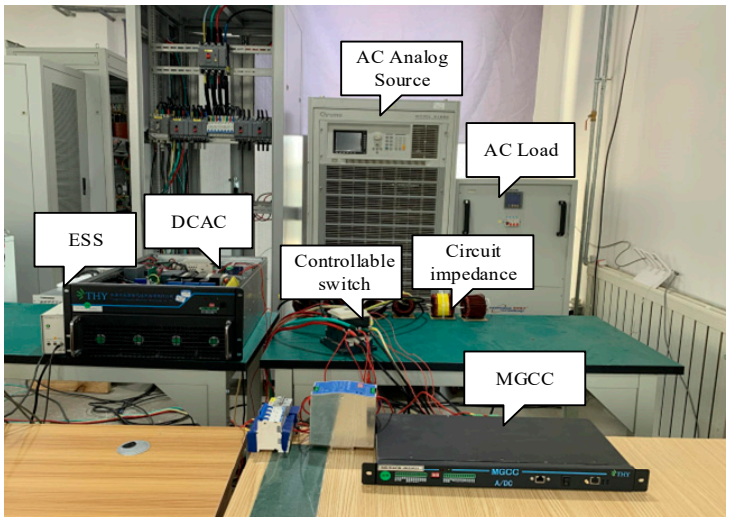

Figure 5. Physical experiment platform.

The specific parameters of the physical experiment are shown in the Table 3 below. The converter used is a T-type three-level single-stage system. Sampling, communication, and main control program calculations are implemented using the digital signal-processing chip TMS320F28335 (Texas Instruments, Dallas, TX, USA). On the DC side, the experiment uses the TC.P.32.1000.400.S.HMI DC analog source (TopCon, Tokyo, Japan) and the G5.54.1000WA000 DC analog source (Regatron, Rorschach, Swiss Confederation). The AC analog source used is the MODEL 61860 AC analog source (Chroma, Xiamen, China). The coordination controller also employs the TMS320F28335 digital signal-processing chip for sampling, communication, and main control program calculations. It can achieve synchronous grid connection functioning with the controlled grid connection switch. Communication in the experiment uses Controller Area Network (CAN) communication.

In the actual physical experiment, a physical circuit identical to the schematic diagram in Figure 3 was constructed. A synchronization coordination controller was set up to sample the values and calculate the compensation values on both sides of the grid connection point. When the voltages on both sides of the grid connection point met the requirements, the controllable switch was closed to achieve grid connection by sending a triggering signal. Meanwhile, to simulate weak communication conditions, compensation information was sent only once.

A synchronization coordination controller was set up to emit pulse signals, u_{sign}, at the beginning and end of the synchronization process. The time consumed for synchronization could be calculated by collecting signals using a recording instrument. This allowed for a comparison of the time taken for synchronization using the passive synchronization

algorithm versus the accelerated synchronization algorithm under the same conditions. It was observed from the combined simulation and experimental results that the conditions where the passive synchronization algorithm took longer were typically those with lower loads, i.e., where the grid-side frequency and microgrid-side frequency were relatively close. Therefore, an AC load of 3 kW was chosen as Experimental Condition 1, while an AC load of 6 kW was chosen as Experimental Condition 2 to compare the time required for synchronization with different synchronization algorithms. The specific experimental results are shown in Figures 6 and 7 and summarized in Table 4.

Table 3. Converter parameters in the physical experiment.

Module	Parameters	Parameters	Symbols	Data
T-type three-level inverter	Hardware System	Filter inductor parameters	L_{p_vsg}	350 μH
		Filter capacitor parameters	U_{thr}	5 V
		Filter capacitor parameters	θ_{thr}	0.1 rad
		DC bus capacitor	$T_{s\_DC/DC}$	66.67 μs
	Control System	Normalized angular frequency	ω_{acB}	314 rad/s
		Voltage per unit	U_{acB}	230 V
		Current per unit	I_{acB}	107 A
		Power per unit	P_{acB}	50 kW
		Primary frequency control parameters for virtual synchronous control	D_{vsg}	50
		Virtual inertia parameters for virtual synchronous control	H_{vsg}	1
		Processing cycle	$T_{s\_DC/AC}$	66.67 μs
Grid connection system	Hardware System	DC bus voltage	u_{C1C2}	750 V
		Line inductance value	L_{line_use}	1.8 mH

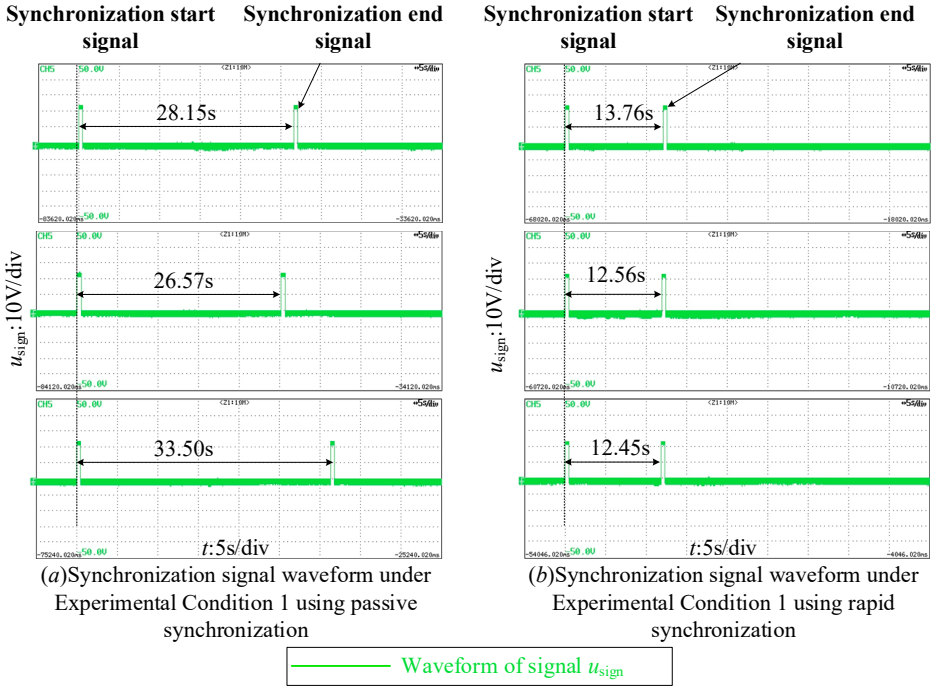

Figure 6. Results of Experiment Condition 1.

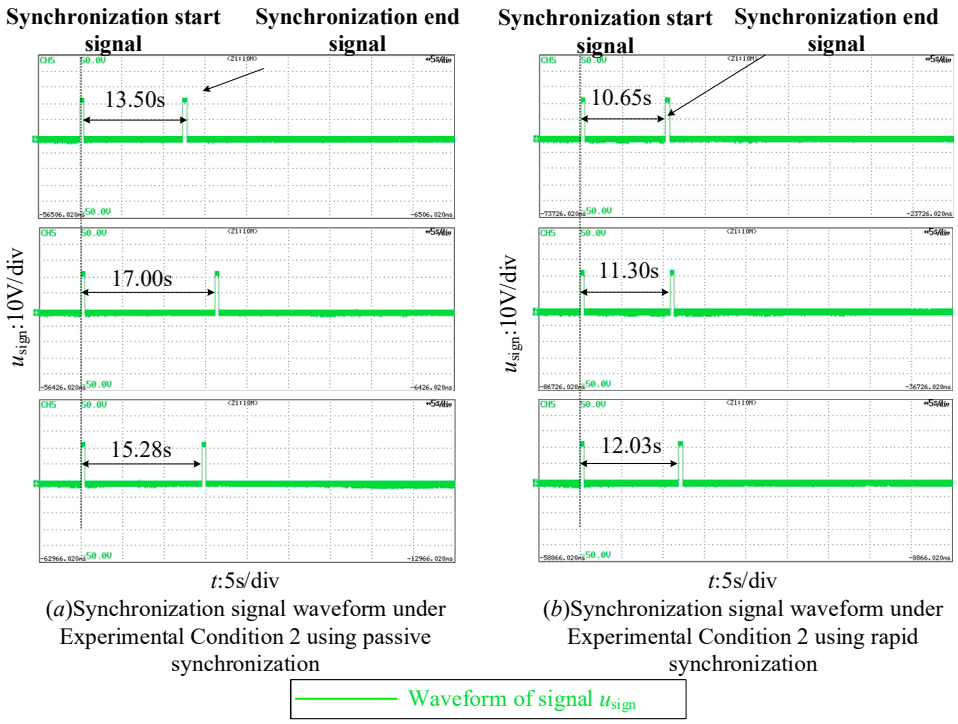

Figure 7. Results of Experiment Condition 2.

Table 4. Results of the single-generator physical experiment.

Simulation Conditions	AC Load	Time for Passive Synchronization	Time for Fast Synchronization	Acceleration Ratio
Experimental Conditions 1	3 kW	28.15 s	13.76 s	51.12%
		26.57 s	12.56 s	52.73%
		33.50 s	12.45 s	62.84%
Average time		29.41 s	12.92 s	56.07%
Experimental Conditions 2	6 kW	13.50 s	10.65 s	21.11%
		17.00 s	11.30 s	33.53%
		15.28 s	12.03 s	21.27%
Average Time		15.26 s	11.33 s	25.75%

Based on the experimental results shown in the Figure 6, Figure 7 and Table 4, the following conclusions can be drawn:

(1) Under a load of 3 kW, the average time taken using the passive synchronization algorithm was 29.41 s, while the average time taken using the fast synchronization algorithm was 12.92 s, which is 43.93% of the time taken by the passive synchronization method. Additionally, due to the uncertainty in the initial phase angle difference at the start of synchronization, the time required for synchronization showed significant randomness. The variance in the synchronization time using the passive synchronization algorithm was 13.1906, while it was only 0.5280 for the fast synchronization algorithm under the same conditions.

(2) Under a load of 6 kW, the synchronization time using the passive synchronization algorithm was 15.26 s, whereas the average time using the fast synchronization method was 11.33 s, which is 74.25% of the time taken by the passive synchronization method. The variance in the synchronization time using the passive synchronization algorithm was 3.0628, while it was only 0.4766 for the fast synchronization algorithm under the same conditions.

This validates the simulation results, showing that when the frequency difference is small, the fast synchronization algorithm is more effective in accelerating the synchronization process and reducing randomness. However, when the frequency difference is large, the acceleration effect and the ability to reduce the randomness of the fast synchronization algorithm are less pronounced.

Subsequently, one inverter was expanded to three identical inverters, connected in parallel through the AC side and integrated into a CAN communication bus to receive information collectively. This configuration formed a three-inverter parallel physical platform, as depicted in Figure 7, to validate the effectiveness of the proposed fast synchronization method under three-inverter operating conditions. The three inverters used the same configuration and control parameters as in the single-inverter physical experiment. The MGCC was set up to calculate compensation values and transmit compensation information, with the compensation value sent only once. An AC load of 9 kW was selected as the operating condition for experiment three, comparing the time required for synchronization using the passive synchronization algorithm and the accelerated synchronization method. The results of the three-inverter physical experiment are illustrated in Figure 8, and a summary of the physical experiment results is presented in Table 5 below.

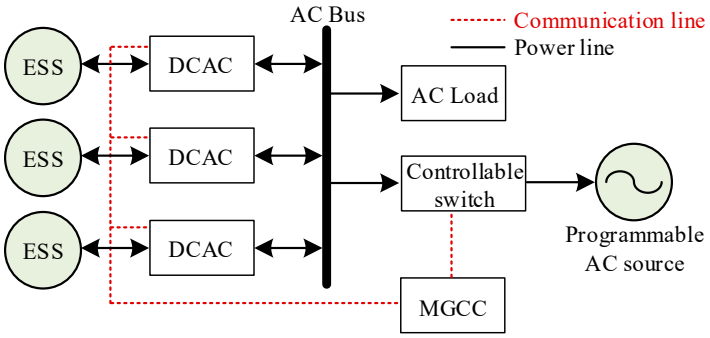

Figure 8. Results of Experimental Conditions 3.

Table 5. Results of the three-generator physical experiment.

Experimental Conditions	AC Load	Time for Passive Synchronization	Time for Fast Synchronization	Acceleration Ratio
Experimental Conditions 3	9 kW	48.34 s	11.65 s	75.90%
		89.56 s	10.93 s	87.80%
		38.35 s	11.10 s	71.06%
Average time		58.75 s	11.23 s	80.89%

Based on the experimental results shown in Figure 9 and Table 5, the following conclusions can be drawn:

(1) Under a load of 9 kW, the average time taken using the passive synchronization algorithm was 58.75 s, while the average time using the fast synchronization algorithm was 11.23 s, which is 19.11% of the time taken by the passive synchronization method.

(2) The variance in the synchronization time when using the passive synchronization algorithm was 736.8921, whereas it was only 0.1416 for the fast synchronization algorithm under the same conditions. This demonstrates that the proposed fast synchronization algorithm significantly reduces the randomness in the time required for synchronization.

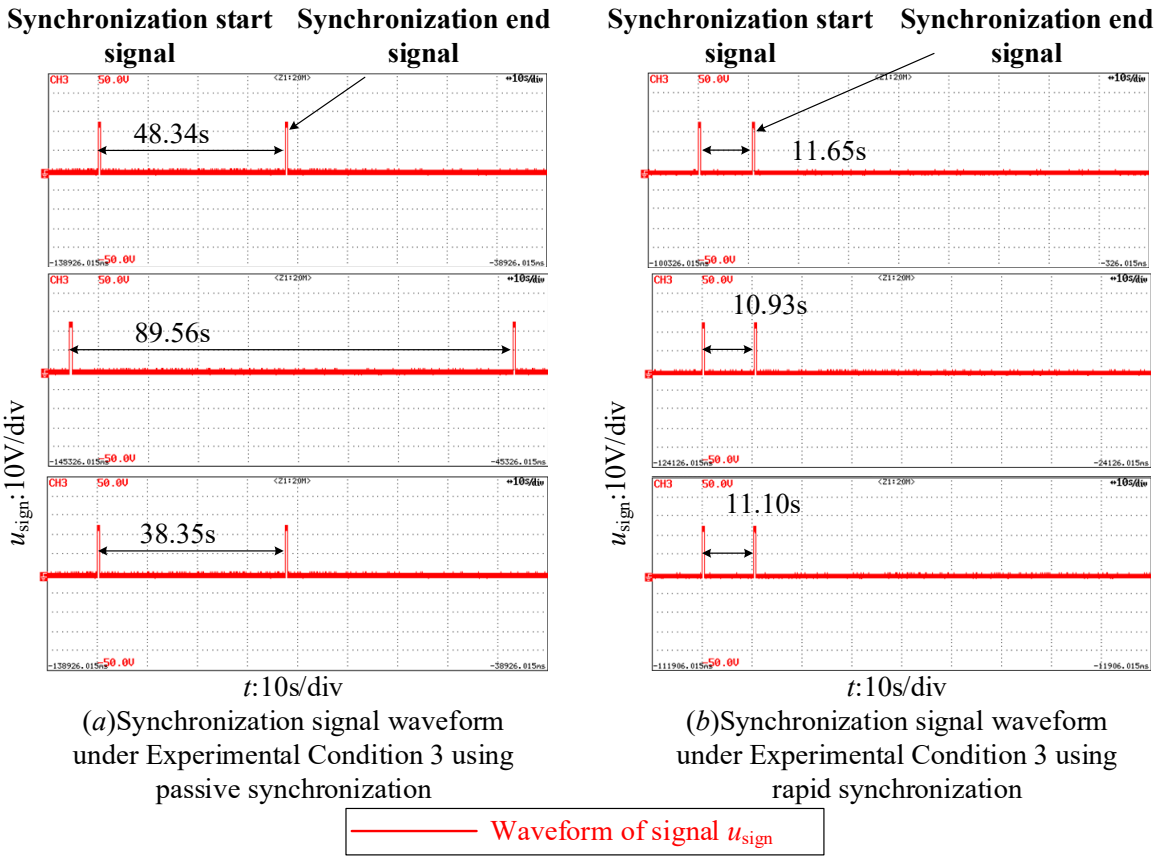

(*a*)Synchronization signal waveform under Experimental Condition 3 using passive synchronization

(*b*)Synchronization signal waveform under Experimental Condition 3 using rapid synchronization

Figure 9. Results of the three-generator physical experiment.

These results validate the simulation conclusions, showing that when the frequency difference is small, the fast synchronization algorithm is more effective. However, when the frequency difference is large, the effectiveness of the fast synchronization algorithm decreases. It can be seen that for multi-machine systems, the proposed fast synchronization method can effectively increase the synchronization speed under weak communication conditions and ensure the normal connection and disconnection of the overall system with the grid.

In conclusion, the experiments effectively validated the simulation results and demonstrated the effectiveness of the proposed fast synchronization algorithm in both single-machine and multi-machine scenarios.

5. Conclusions

This paper presents a fast synchronization method based on actively increasing the frequency difference between the two sides of the grid connection point. It analyzes and summarizes the selection methods for several key control parameters in this method. Finally, the effectiveness of the proposed approach is validated through PSCAD/EMTDC and physical experiments.

The main conclusions of this paper can be summarized as follows:

1. To address the issue of systems using grid-forming control under weak communication conditions being unable to quickly adjust their frequency and phase angle, a fast synchronization method is proposed. This method compensates for synchronization based on the frequency difference between the two sides of the grid connection point, actively increasing the frequency difference between the two sides to reduce the time required for the synchronization process. It also minimizes the impact of communication resource usage and communication delays. Finally, the effectiveness

of the proposed fast synchronization algorithm is validated through simulation and physical experiment results.

2. For the proposed fast synchronization method, an analysis was conducted on the key control parameters' value ranges based on synchronization grid connection thresholds. Corresponding methods and ranges for selecting control parameters were summarized. Finally, a set of classic control parameter values was presented, and the effectiveness of this set of control parameters was validated through simulation and experimental results.

These conclusions demonstrate the practical viability and advantages of the fast synchronization method proposed in this paper.

Author Contributions: Supervision, J.L.; project administration, H.L. and F.L.; writing—original draft, Y.H.; conceptualization, X.L. All authors have read and agreed to the published version of the manuscript.

Funding: This research was funded by [Guangdong Power Grid Co., Ltd.] grant number [030600KK52222013(GDKJXM20222579)].

Data Availability Statement: The original contributions presented in the study are included in the article, further inquiries can be directed to the corresponding author.

Conflicts of Interest: Authors Jiangang Lu, Haobin Li, Feng Liao, Yuhui Huang were employed by the company Guangdong Power Grid Co., Ltd. The remaining authors declare that the research was conducted in the absence of any commercial or financial relationships that could be construed as a potential conflict of interest.

References

1. Shair, J.; Li, H.; Hu, J.; Xie, X. Power system stability issues, classifications and research prospects in the context of high-penetration of renewables and power electronics. *Renew. Sustain. Energy Rev.* **2021**, *145*, 1364–1378. [CrossRef]
2. Wang, C.; Pu, L.; Du, B.; Wan, Z.; Zhang, J.; Zhao, Z. Novel Fuzzy Adaptive Inertia Based Virtual Synchronous Generator for Microgrid Frequency Fluctuation Attenuation. *Electr. Drive* **2022**, *52*, 14–20.
3. Chai, J.; Zhao, Y.; Sun, X.; Geng, H. Application and Prospect of Virtual Synchronous Generator in Wind Power Generation System. *Autom. Electr. Power Syst.* **2018**, *42*, 17–25.
4. Blaabjerg, F.; Teodorescu, R.; Liserre, M.; Timbus, A.V. Overview of control and grid synchronization for distributed power generation systems. *IEEE Trans. Ind. Electron* **2006**, *53*, 1398–1409. [CrossRef]
5. Tang, X.; He, Y.; Li, Z.; Li, X. Frequency Division Compensation Method for Phase Margin of Grid Connected Converters in the Weak Grid. *Proc. CSEE* **2024**, *44*, 1565–1575.
6. Liu, H.; Fang, T.; Zhang, H.; Zhu, Y. Research on an Improved Voltage Feedforward Path of Grid-Connected Inverter Coping with Complex Stability Issues in Weak Grid. *Trans. China Electrotech. Soc.* **2024**, *39*, 4955–4967.
7. Ge, P.; Tu, C.; Xiao, F.; Guo, Q. Transient Stability Enhancement of a VSG Based on Flexible Switching of Control Parameters. *Proc. CSEE* **2022**, *42*, 2109–2124.
8. Hang, H.; Wang, Y.; Liu, Y.; Yang, P.; Li, M.; Lei, W. The LVRT Strategy for VSG Based on the Quantitatively Designed Virtual Impedance. *High Volt. Eng.* **2022**, *48*, 245–256.
9. Zhang, Y.; Zhao, J.; Li, F.; Mao, L.; Li, J.; Qi, W. VSG Fault Crossing Method Based on Dynamic Compensation of Power Angle. *Power Syst. Technol.* **2021**, *45*, 3667–3673.
10. Xu, W.; Wang, L.; Bai, Y.; He, S. Research on Frequency and Smooth Switching Control of Microgrid System Based on Fuzzy Droop Control. *J. Power Supply.* **2022**. Available online: https://kns.cnki.net/kcms/detail/12.1420.TM.20220328.1213.002.html (accessed on 6 November 2024).
11. He, X.; Geng, H.; Xi, J.; Guerrero, J.M. Resynchronization Analysis and Improvement of Grid-Connected VSCs During Grid Faults. *IEEE J. Emerg. Sel. Top. Power Electron.* **2021**, *9*, 438–450. [CrossRef]
12. Sahoo, A.K.; Mahmud, K.; Crittenden, M.; Ravishankar, J.; Padmanaban, S.; Blaabjerg, F. Communication-Less Primary and Secondary Control in Inverter-Interfaced AC Microgrid: An Overview. *IEEE J. Emerg. Sel. Top. Power Electron.* **2021**, *9*, 5164–5182. [CrossRef]
13. Del Carpio Huayllas, T.E.; Ramos, D.S.; Vasquez-Arnez, R.L. Microgrid systems: Current status and challenges. In Proceedings of the 2010 IEEE/PES Transmission and Distribution Conference and Exposition: Latin America (T&D-LA), Sao Paulo, Brazil, 8–10 November 2010; pp. 7–12.
14. Zhou, P.; Zhang, X.; Di, Q.; Yue, J. Pre-synchronous Grid-connection Strategy of DFIG-based Wind Turbine with Virtual Synchronous Generator Control. *Autom. Electr. Power Syst.* **2020**, *44*, 71–78.

15. Zheng, W.; Liu, L.; Zeng, J. Smooth Switching Strategy Between Grid-Connected and Islanded Microgrid Using Improved Phase Control Method. *Power Syst. Technol.* **2016**, *40*, 1155–1162.
16. Amin, M.; Zhong, Q. Resynchronization of distributed generation based on the universal droop controller for seamless transfer between operation modes. *IEEE Trans. Ind. Electron.* **2020**, *67*, 7574–7582. [CrossRef]
17. Guo, H.; Meng, X.; He, M.; Liu, X.; Liu, J. An Enhanced Power Quality and Smooth Transition Control Strategy for a Microgrid without Remote Pre-Synchronization Communication. *Trans. China Electrotech. Soc.* **2022**, *37*, 2611–2621.
18. Kumar, S.; Singh, B. Seamless operation and control of single phase hybrid PV-BES-utility synchronized system. *IEEE Trans. Ind. Appl.* **2019**, *55*, 1072–1082. [CrossRef]
19. Huang, S.; Konishi, Y.; Yang, Z.; Hsieh, M. Observer-based capacitor current sensorless control applied to seamless transfer single-phase inverter System. *IEEE Trans. Power Electron.* **2019**, *34*, 2819–2828. [CrossRef]
20. Huang, Q.; Cao, S.; Wu, Y.; Lin, X.; Wei, F.; Yang, D.; Cui, T. A New Multi-infeed Short Circuit Ratio Index Taking Into Account the Amplitude and Phase Characteristics of New Energy. *Proc. CSEE* **2024**, *44*, 5960–5972.
21. *IEEE 1204-1997*; IEEE Guide for Planning DC Links Terminating at AC Locations Having Low Short-Circuit Capacities. IEEE: New York, NY, USA, 1997.
22. Li, X.; Wang, Z.; Guo, L.; Zhu, L.; Zhu, J.; Fu, X.; Zhang, Y.; Wang, C. Transient Stability Analysis of PLL Synchronization in Weak-grid-connected VSCs Based on the Largest Estimated Domain of Attraction. *Proc. CSEE* **2022**, *42*, 7485–7496.
23. Yang, X. Research on Microgrid Inverter and Coordinated Control Strategies of Multiinverters. Ph.D. Thesis, Hefei University of Technology, Hefei, China, 2011.
24. Zhang, H.; Cai, X.; Lu, G. Generator quasi synchronization parameter measurement method based on improved phase difference method of all-phase fast Flourier transform. *Power Syst. Prot. Control* **2016**, *44*, 76–83.
25. Meng, L.; Hu, X.; Xiao, G.; Gao, Z.; Ji, P. On-line measurement method of grid impedance based on grid-connected inverter under frequency fluctuate. *Electr. Power Autom. Equip.* **2024**, 149–156. [CrossRef]